Metal-insulator transition and local-moment collapse in negative charge transfer $CaFeO_3$ under pressure

I. Leonov

M. N. Miheev Institute of Metal Physics, Russian Academy of Sciences, 620108 Yekaterinburg, Russia and Ural Federal University, 620002 Yekaterinburg, Russia

(Received 1 October 2021; revised 16 December 2021; accepted 21 January 2022; published 31 January 2022)

We compute the electronic structure, spin and charge state of Fe ions, and the structural phase stability of paramagnetic $CaFeO_3$ under pressure using a fully self-consistent in charge density DFT + dynamical mean-field theory method. We show that at ambient pressure $CaFeO_3$ is a negative charge transfer insulator characterized by strong localization of the Fe $3d$ electrons. It crystallizes in the monoclinic $P2_1/n$ crystal structure with a cooperative breathing mode distortion of the lattice. While the Fe $3d$ Wannier occupations and local moments are consistent with robust charge disproportionation of Fe ions in the insulating $P2_1/n$ phase, the physical charge density difference around the structurally distinct Fe A and Fe B ions with the "contracted" and "expanded" oxygen octahedra, respectively, is rather weak, of ∼0.04. This implies the importance of the Fe $3d$ and O $2p$ negative charge transfer and supports the formation of a bond-disproportionated state characterized by the Fe A $3d^{5-\delta}\underline{L}^{2-\delta}$ and Fe B $3d^5$ valence configurations with $\delta \ll 1$, in agreement with strong hybridization between the Fe $3d$ and O $2p$ states. This complex interplay between electronic correlations, strong covalency, and lattice effects, resulting in bond disproportionation, is in many ways reminiscent of the behavior of rare-earth nickelates, RNiO$_3$ (R = rare earth). Upon compression, $CaFeO_3$ undergoes the metal-to-insulator phase transition (MIT) which is accompanied by a structural transformation into the orthorhombic $Pbnm$ phase. The phase transition is accompanied by suppression of the cooperative breathing mode distortion of the lattice and, hence, results in the melting of bond disproportionation of the Fe ions. Our analysis suggests that the MIT transition is associated with orbital-dependent delocalization of the Fe $3d$ electrons and leads to a remarkable collapse of the local magnetic moments. Our results imply the crucial importance of the interplay of electronic correlations and structural effects to explain the properties of $CaFeO_3$.

DOI: 10.1103/PhysRevB.105.035157

I. INTRODUCTION

The transition metal oxides with perovskite crystal structure have attracted much attention due to their diverse electronic and magnetic properties, allowing for a broad range of applications, e.g., in electronics and spintronics, and energy storage [1–6]. A particular interest is given to the understanding of a Mott metal-insulator transition (MIT) driven by correlation effects, the description of which has been a long-standing challenge [1,2]. In this context metal oxides with an unusually high valence state of the transition metal, Ni^{3+} (nickelates) and Fe^{4+} (ferrates), are notable because of a complex interplay of ligand holes and electronic correlations in the $3d$ shell of Ni and Fe ions [7–13], which leads to their complex physical behavior.

Such materials are often regarded as "negative charge transfer" compounds, implying the importance for a charge transfer from oxygen to the transition metal atom, leaving holes at oxygen ligands, to explain their electronic properties [14,15]. In particular, the rare-earth nickelate perovskites RNiO$_3$ (R = rare earth, R^{3+}) with a high oxidation state of nickel, Ni^{3+} $3d^7$ (with a nominal Ni $t_{2g}^6e_g^1$ electron configuration) exhibit a sharp metal-insulator transition (except for LaNiO$_3$) upon cooling and under pressure [11–13,16,17]. The MIT transition is accompanied by a structural transformation from the orthorhombic metallic ($Pbnm$, distorted GdFeO$_3$ type) to monoclinic insulating ($P2_1/n$) crystal structure, with a cooperative breathing mode distortion of NiO_6 octahedra in the insulating $P2_1/n$ phase [16,17]. While analysis of the Ni-O bond lengths and x-ray absorption spectroscopy suggests charge disproportionation of Ni ions in the insulating RNiO$_3$ phases, their electronic state is more accurately described in terms of bond disproportionation, with alternating Ni ions which (nearly) adopt a Ni^{2+} $3d^8$ (Ni^{2+} ions with local moments) and $3d^8\underline{L}^2$ (nonmagnetic spin singlet) electronic configuration ($\underline{L}$ denotes a hole in the O $2p$ band) [18–27]. We also note that the complex interplay between (negative) charge transfer and correlation effects can result in unusual charge or bond disproportionation of the A-site ions of the perovskite ABO_3 structure, e.g., in BiNiO$_3$ [28–34], PbFeO$_3$ [35,36], and PbCoO$_3$ [37–39].

In the present work, we focus on a negative charge transfer material $CaFeO_3$ with a nominal Fe $3d^4$ ($t_{2g}^3e_g^1$) electronic state which exhibits the MIT upon cooling below ∼290 K (at ambient pressure) [9–13]. Moreover, the MIT occurs upon compression of $CaFeO_3$ above ∼30 GPa [7]. It shows a complex screw antiferromagnetic structure below the Néel temperature ∼115 K [9,10]. Similarly to the rare-earth

nickelates, the MIT in $CaFeO_3$ is accompanied by a structural transformation from the orthorhombic metallic (*Pbnm*) to monoclinic insulating ($P2_1/n$) crystal structure, with a cooperative breathing mode distortion of FeO_6 octahedra with the difference in Fe-O bond lengths ∼0.1 Å in the insulating $P2_1/n$ phase [9,10]. We note however that in contrast to the rare-earth nickelates, in $CaFeO_3$ a nominal Fe^{4+} $t_{2g}^3 e_g^1$ electron configuration yields a half-filled (magnetic) Fe t_{2g} band. This leads to the five-orbital effective degeneracy of low-energy excitations, implying the importance of the interband t_{2g}-e_g correlation effects in $CaFeO_3$. The latter are negligible in $RNiO_3$ in which the Ni t_{2g} states are fully occupied (and nonmagnetic). Moreover, this leads to an addition complexity of the electronic structure of $CaFeO_3$ under pressure associated with the interplay between the high-spin and low-spin states of Fe ions.

Given the electronic and structural complexity of $CaFeO_3$ (e.g., doped with Ca and La) and its similarity to the rare-earth nickelates, this system has been intensively studied using both experimental and theoretical methods [7–10,40–56]. Previous calculations were mostly employed band-structure methods supplemented with the on-site Coulomb correlations for the Fe 3*d* states within density functional theory (DFT) $+U$ method [57,58] with a major focus on the ground state properties of the insulating $P2_1/n$ phase with a long-range magnetic ordering [49–53]. Using the DFT+U and more advanced strongly constrained appropriately normed exchange and correlation functional (SCAN) methods [57–59] the authors address the questions about the origin of a band gap, charge and bond disproportionation, ligand hole effects, Mott vs charge transfer insulator behaviors, etc., in $CaFeO_3$ [54–56]. We note however that although the static mean-field DFT+U and SCAN methods can be useful to explain many of the (static) properties of strongly correlated electron materials (presumably with a long-range magnetic order), these techniques by construction neglect electron dynamics (one-electron approximation) and hence cannot capture correlated electron phenomena related to the Mott MIT such as a coherence-incoherence crossover, quasiparticle behavior, and strong (orbital-selective) quasiparticle mass renormalizations.

Recently, the electronic structure of $CaFeO_3$ has been discussed [60] in the context of a five-orbital tight-binding model using the DFT+dynamical mean-field theory (DFT+DMFT) method [61–68]. DFT+DMFT has been proven to be among the most advanced theoretical methods for studying the electronic properties of strongly correlated materials, such as correlated transition metal oxides, heavy fermions, and Fe-based superconductors, e.g., to study the Mott metal-insulator phase transition, collapse of local moments, large orbital-dependent renormalizations, etc. [65–92]. The DFT+DMFT results for the tight-binding model [60] show the competition between high-spin and low-spin homogeneous and an inhomogeneous charge-disproportionated state, implying the importance of Hund's coupling [93–96]. Nonetheless, the electronic properties of $CaFeO_3$ and, in particular, the interplay of the electronic structure, magnetic states, and phase stability of $CaFeO_3$ near the MIT are still poorly understood.

We address this problem in our study by using a fully self-consistent in charge density DFT+DMFT method [65–71] implemented with plane-wave pseudopotentials [97]. In particular, we explore the electronic structure, magnetic properties, spin and charge state of Fe ions, and structural phase stability of *paramagnetic* $CaFeO_3$ near the pressure-induced MIT. Our results show the importance of the Fe 3*d* and O 2*p* negative charge transfer due to strong covalency and support the formation of the bond-disproportionated state in the insulating phase of $CaFeO_3$. This complex interplay of charge transfer and electronic correlations in the 3*d* shell of Fe ion is in many ways reminiscent of the behavior of rare-earth nickelates.

II. METHOD

We employ the state-of-the-art DFT+DMFT method [62–64] with full self-consistency over the charge density [65–71] to explore the electronic structure, spin and charge state of Fe ions, and lattice properties of paramagnetic $CaFeO_3$ under pressure. For simplicity, to model pressure effects we adopt the crystal structure parameters determined experimentally for the monoclinic $P2_1/n$ phase (at ambient pressure and temperature ∼15 K) and for the orthorhombic *Pbnm* structures (taken above the insulator-to-metal and charge-disproportionation transition, at 300 K) [9,10], and evaluate the DFT+DMFT total energies as a function of the unit-cell volume (keeping fixed all the internal crystal structure parameters of the $P2_1/n$ and *Pbnm* phases) [69–71]. We fit the total-energy results using the third-order Birch-Murnaghan equation of states separately for the low- and high-volume regions [98,99].

We start by constructing the effective low-energy Hamiltonian for the partially occupied Fe 3*d* and O 2*p* states and consider the multiorbital Hubbard Hamiltonian with the local electron-electron interaction part for the Fe 3*d* orbitals

$$\hat{H}_{\rm int} = \frac{1}{2}\sum_{mm'\sigma} U_{mm'}\hat{n}_{m\sigma}\hat{n}_{m'\bar{\sigma}} + \frac{1}{2}\sum_{m\neq m'\sigma}(U_{mm'}-J_{mm'})\hat{n}_{m\sigma}\hat{n}_{m'\sigma}, \quad (1)$$

where $\hat{n}_{m\sigma}$ is the occupation number operator with spin σ and (diagonal) orbital indices m. $U_{mm'}$ and $J_{mm'}$ are the Coulomb repulsion and Hund's exchange coupling matrix elements. In Eq. (1) we assume summation over all Fe sites. For the partially filled Fe 3*d* and O 2*p* orbitals we construct a basis set of atomic-centered symmetry-constrained Wannier functions [100–102] (the localized Fe 3*d* orbitals are constructed using the Fe 3*d* band set, while the O 2*p* orbitals were defined over the full energy window spanned by the O 2*p*–Fe 3*d* band complex [103]). This makes it possible to explicitly account for charge transfer effects between the partially occupied Fe 3*d* and O 2*p* states and strong Coulomb correlations of the Fe 3*d* electrons. We use the continuous-time hybridization expansion (segment) quantum Monte Carlo algorithm in order to solve the realistic many-body problem [104].

The DFT+DMFT calculations are performed in the paramagnetic (PM) state at an electronic temperature $T = 387$ K. The Coulomb $U_{mm'}$ and Hund's exchange $J_{mm'}$ matrix elements are parametrized in terms of the Slater integrals F_0, F_2, and F_4 which are expressed in terms of the average Coulomb

repulsion $U = F_0$ and Hund's exchange coupling $J_H = (F_2 + F_4)/14$, with a fixed ratio $F_4/F_2 = 0.63$. We take the average Hubbard $U = 6$ eV and Hund's exchange $J_H = 0.86$ eV in accordance with previous DFT+DMFT studies [91,92]. The fully localized double-counting correction evaluated from the self-consistently determined local occupations was used, $\hat{H}_{\rm DC} = U(N - \frac{1}{2}) - J(N_\sigma - \frac{1}{2})$, where N_σ is the total Fe $3d$ occupation with spin σ and $N = N_\uparrow + N_\downarrow$. The Coulomb interaction is treated in the density-density approximation, neglecting spin-flip and pair-hopping terms in the multiorbital Hubbard Hamiltonian. The spin-orbit coupling is neglected in our calculations. The spectral functions were computed using the maximum entropy method. In order to estimate the quasiparticle mass enhancement m^*/m of the Fe $3d$ states we perform analytic continuation of the self-energy $\Sigma(\omega)$ determined self-consistently on the Matsubara contour using Padé approximants. In order to analyze a degree of localization of the Fe $3d$ electrons we compute the local spin susceptibility $\chi(\tau) = \langle \hat{m}_z(\tau)\hat{m}_z(0)\rangle$ within DMFT, where $\hat{m}_z(\tau)$ is the instantaneous magnetization on the Fe $3d$ site at the imaginary time τ (τ denotes an imaginary-time evolution ranging from 0 to $\beta = 1/k_BT$ in the path integral formalism).

In DFT we use the generalized gradient Perdew-Burke-Ernzerhof approximation for the correlation exchange functional [105], with the ultrasoft pseudopotential (USPP) with the nonlinear core correction for Fe (Fe.pbe-nd-rrkjus.UPF), USPP for O (O.pbe-rrkjus.UPF), and GBRV version 1.4 USPP for Ca [97,106–109]. In the DFT calculations we use the kinetic energy cutoffs for the wave functions of 45 Ry and for the charge density and potentials of 650 Ry.

III. RESULTS AND DISCUSSION

A. Electronic structure and phase stability of $P2_1/n$ $CaFeO_3$ at low pressures

We start by computing the electronic properties and structural phase stability of PM $CaFeO_3$ under pressure. Our results for the total energy calculations and compressional behavior of $CaFeO_3$ are summarized in Fig. 1. The $P2_1/n$ phase is found to be energetically favorable, i.e., thermodynamically stable at ambient pressure, with a total-energy difference of ∼13 meV/atom with respect to the *Pbnm* phase. This implies that at low pressure and temperature conditions $CaFeO_3$ crystallizes in the $P2_1/n$ phase which is characterized by the cooperative breathing-mode distortion of the crystal structure, in agreement with the x-ray and neutron diffraction experiments [9,10]. The calculated equilibrium lattice volume for the $P2_1/n$ phase is $V_0 = 375.4$ a.u.^{3} (by ∼4% larger than that in the experiment) and bulk modulus $K_0 = 151$ GPa (with $K' \equiv dK/dP$ fixed to $K' = 4.0$). Our results for the instantaneous magnetic moments of the structurally distinct Fe A and Fe B sites with the "contracted" and "expanded" oxygen octahedra, respectively, are 3.18 and 4.65 μ_B (see Fig. 2). These values are close to the calculated fluctuating moments ∼2.98 and 4.58 μ_B, evaluated as the imaginary-time average of local spin susceptibility $\chi(\tau) = \langle \hat{m}_z(\tau)\hat{m}_z(0)\rangle$, $m_{\rm loc} = [k_BT \int \chi(\tau)d\tau]^{1/2}$. This suggests strong localization of the Fe $3d$ electrons at low pressures, implying the crucial importance of electronic correlations to explain the electronic properties

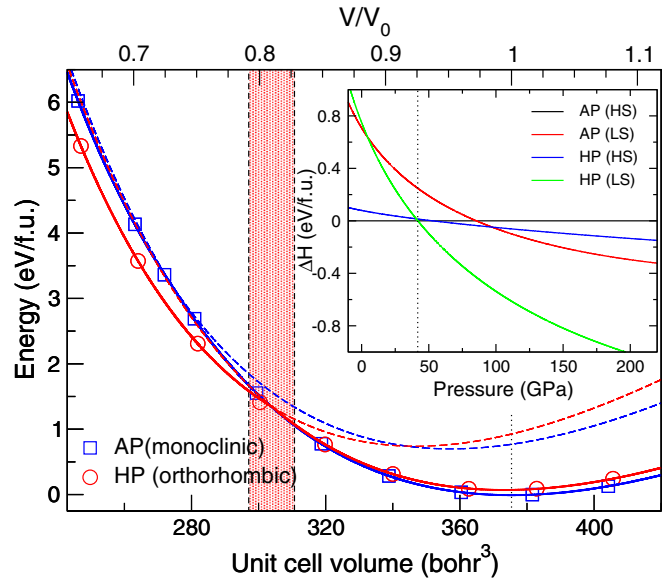

FIG. 1. Total energy of PM $CaFeO_3$ calculated by DFT+DMFT at $T = 387$ K as a function of lattice volume. The lattice volume collapse associated with the $P2_1/n$-*Pbnm* structural phase transition (the lattice volume difference at the common pressure) is depicted by red shading. Inset: Enthalpy difference (relative to the high-spin $P2_1/n$ solution) obtained by DFT+DMFT as a function of pressure. The $P2_1/n$-*Pbnm* structural transition at ∼41 GPa is shown by a vertical dotted line.

of $CaFeO_3$. We also note that the calculated local moments are in good agreement with the experimental estimates of 2.5–3.5 μ_B and 3.5–5.0 μ_B for the Fe A and B sites obtained from the fit of neutron diffraction data using different spiral

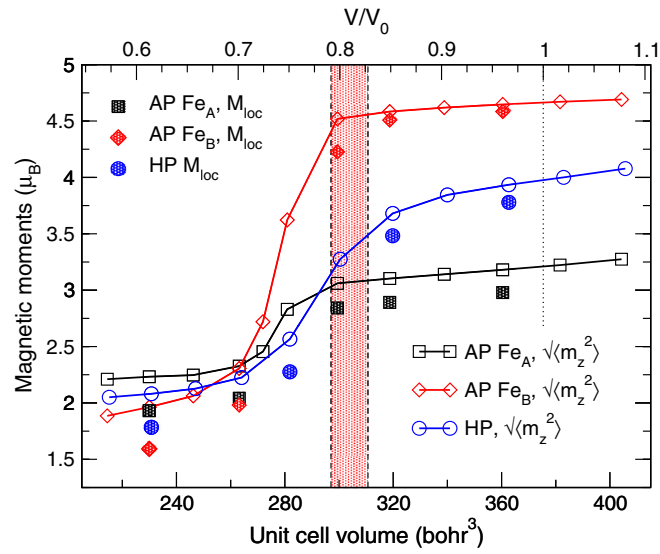

FIG. 2. The local magnetic moments of the ambient-pressure $P2_1/n$ (AP) and high-pressure *Pbnm* (HP) structural phases of PM $CaFeO_3$ obtained by DFT+DMFT at $T = 387$ K as a function of the unit-cell volume. The unit-cell volume collapse associated with the MIT and the $P2_1/n$-*Pbnm* structural transition is depicted by red shading.

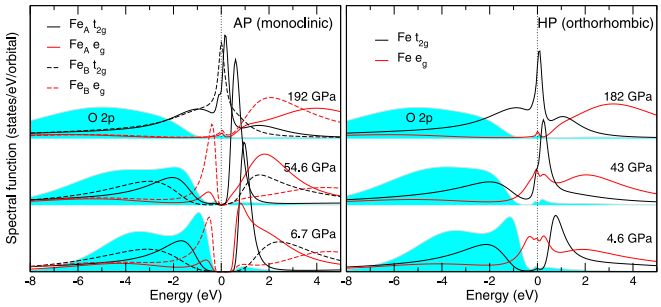

FIG. 3. Orbitally resolved spectral functions of PM $CaFeO_3$ calculated by DFT+DMFT for the $P2_1/n$ (left panel) and *Pbnm* (right panel) phases for different lattice volumes.

magnetic structures [9,10]. We note that in the DFT+U and SCAN calculations the magnetic moments are 3.42/3.85 μ_B and 2.66/3.72 μ_B, respectively [55,56].

B. Spectral function and spin state of iron

In agreement with experiment, we obtain a negative charge transfer insulator [14,15] with an energy gap of ∼0.6 eV (see the left panel of Fig. 3). Our results for the orbitally resolved spectral functions of PM $CaFeO_3$ are shown in Fig. 3. The energy gap lies between the occupied Fe B e_g states strongly mixed with the O $2p$ and the unoccupied Fe A $3d$ states. The latter strongly hybridize with the empty O $2p$ states. The occupied O $2p$ band appears at about −6 eV to near the Fermi level. The top of the valence band has a strongly mixed Fe $3d$ and O $2p$ character, with a resonant peak in the filled Fe e_g states located at about −0.4 eV below the Fermi level. This behavior can be ascribed to the formation of a Zhang-Rice bound state [110].

Fe t_{2g} and e_g Wannier orbital occupancies are 0.55 and 0.25 per spin orbit for the Fe A and are 0.52 and 0.5 for the Fe B ions, respectively. These findings clearly indicate that at ambient pressure the Fe B ions are in the high-spin (HS) state. In fact, in an ionic picture, the Fe^{3+} ions have a $3d^5$ configuration with three electrons in the t_{2g} and two in the e_g orbitals (in the octahedral crystal field), forming the $S = 5/2$ state. This result is in agreement with our results for the decomposition of the electronic state into atomic spin state configurations within DFT+DMFT. In particular, for the Fe B ions the HS state has a predominant weight of ∼97% with a small admixture of ∼3% due to the intermediate-spin (IS) state in the insulating $P2_1/n$ phase (at ambient pressure). On the other hand, the Fe A ions show a strong mixture of the HS and IS state configurations whose corresponding weights are ∼ 47% and 43%.

C. Fe 3*d* Wannier orbital occupancies and bond disproportionation

Moreover, our analysis of the Fe $3d$ Wannier occupations give a remarkable charge disproportionation between the Fe A and Fe B sites (due to a sufficiently different oxygen environment of these sites in the insulating $P2_1/n$ phase, with the difference in Fe-O bond lengths ∼0.1 Å [9,10]). In fact, at ∼6.7 GPa the total Fe $3d$ Wannier occupation for the Fe A site is only ∼4.3, while for the Fe B sites it is 5.1, implying a rather large charge difference of ∼0.8 electron. We note that this charge difference is about 40% of the ideal ionic Fe^{3+}-to-Fe^{5+} charge disproportionation, roughly consistent with the bond valence sum estimate of ∼1.1 [9,10], as well as is in agreement with the significantly different local magnetic moments for the Fe A and Fe B sites (see above). Interestingly, previous estimates of a charge disproportionation in the low-temperature charge-ordered phases of the mixed-valence oxides such as Fe_3O_4 and rare-earth nickelates $RNiO_3$ give ∼20–40% of the ideal ionic disproportionation [11,16,17,111–116], consistent with our results.

In agreement with this, our analysis of the eigenvalues of the reduced Fe $3d$ density matrix, i.e., an estimate of a fluctuating valence state of Fe ions, shows that the Fe B ions (with "expanded" oxygen octahedra) are 3+. In fact, for the Fe B ions the $3d^5$ configuration has a predominant weight of about 74% with a ∼7% admixture of the $3d^4$ and ∼18% of the $3d^6$ configurations (due to quantum mixing and temperature effects). On the other hand, for the Fe A ions the $3d^4$ and $3d^5$ configurations are nearly equally weighted, of ∼48% and 34%, respectively, in accordance with above estimates. That is, the electronic state of the Fe A ions consists of heavily mixed d^4 and $d^5\underline{L}$ states, reflecting the importance of Fe $3d$ to O $2p$ negative charge transfer due to strong covalency in $CaFeO_3$.

While our results for the Fe $3d$ Wannier occupations and local moments give a robust charge disproportionation in the $P2_1/n$ insulating phase, a difference of the total charge density $\rho(\mathbf{r})$ around the structurally distinct Fe A and Fe B ions is rather weak. In particular, our result for the corresponding charge difference within the Fe-ion radius of 0.86 Å gives an order of magnitude smaller value of ∼0.04 (in fact our estimate is consistent with the results of the previous DFT+U and SCAN calculations [55,56]). This implies the importance of the Fe $3d$ and O $2p$ negative charge transfer and suggests the formation of a bond-disproportionated state characterized by the Fe $3d^{5-\delta}\underline{L}^{2-\delta}$ and $3d^5$ electronic configurations with $\delta \ll 1$ for the "compressed" Fe A and "expanded" Fe B sites, respectively, in the insulating phase of $CaFeO_3$. This result is consistent with a substantial Fe-O covalence and strong hybridization between the unoccupied Fe e_g and O $2p$ state [14,15]. We also note that this behavior is in line with that of the rare-earth nickelate perovskites, $RNiO_3$ [18–27].

D. Pressure-induced Mott MIT and delocalization of the Fe 3*d* electrons

Under pressure the energy gap of $P2_1/n$ $CaFeO_3$ gradually decreases, resulting in an insulator-to-metal phase transition. Within the $P2_1/n$ structure (i.e., by neglecting the structural effects) the MIT occurs upon compression to ∼$0.74V_0$, above ∼85 GPa. The phase transition is accompanied by a remarkable anomaly of our DFT+DMFT total-energy and local-moment results. In fact, the local moments of the Fe A and B ions are significantly different and are seen to retain their high-spin values down to ∼$0.74V_0$, while upon further compression collapse to a nearly same moment value of ∼2.3 μ_B, at 102 GPa. The phase transition is accompanied by a large transfer of the Fe $3d$ spectral weight, with a formation

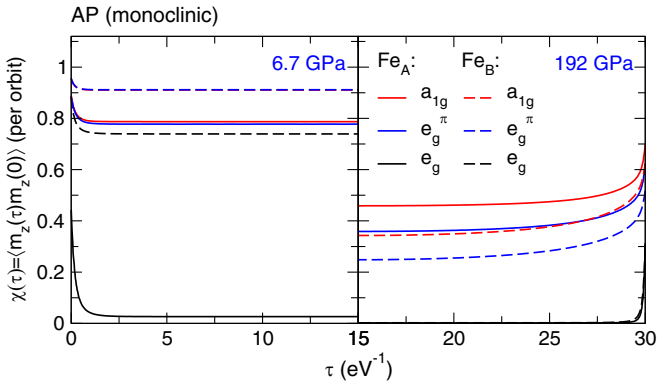

FIG. 4. Orbitally resolved local spin correlations functions $\chi(\tau) = \langle \hat{m}_z(\tau)\hat{m}_z(0)\rangle$ of the $P2_1/n$ phase of $CaFeO_3$ calculated by DFT+DMFT for different pressures.

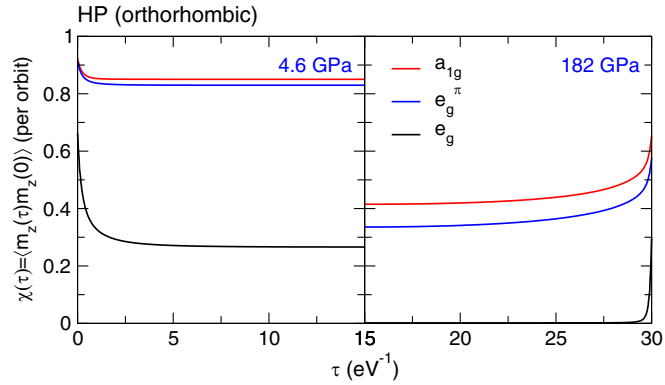

FIG. 5. Orbitally resolved local spin correlations functions $\chi(\tau) = \langle \hat{m}_z(\tau)\hat{m}_z(0)\rangle$ of the *Pbnm* phase of $CaFeO_3$ calculated by DFT+DMFT for different pressures.

of the Fe $3d$ quasiparticle peak near the Fermi level. It is associated with a substantial redistribution of charge within the Fe $3d$ shell. Fe t_{2g} orbital occupations are found to gradually increase with pressure (t_{2g} occupation is about 0.66 per spin orbit for the Fe A and 0.69 for the Fe B sites at 102 GPa). This comes along with a significant depopulation of the Fe e_g states. Fe A and B e_g occupations are 0.17 and 0.19 per spin orbit, respectively, while the Wannier Fe $3d$ total occupancies change to 4.6 and 4.87 for the Fe A and Fe B ions. This implies a significant reduction of charge disproportionation upon metallization of the $P2_1/n$ structure, to about 0.26 at 102 GPa.

Our results for the local (dynamical) spin-spin correlation function $\chi(\tau) = \langle \hat{m}_z(\tau)\hat{m}_z(0)\rangle$ reveal significant delocalization of the Fe $3d$ electrons under pressure as seen in Fig. 4. $\chi(\tau)$ is strongly suppressed, quickly decaying with the imaginary time τ (it is most pronounced for the Fe B e_g states). On the other hand, a relatively large value of $\chi(\tau)$ of $\sim$ 0.3–0.4 μ_B^2 at $\tau \simeq \beta/2$ (with $\beta = 1/k_BT = 30$ eV^{-1} at $T = 387$ K) for the Fe A and B t_{2g} states suggests the proximity of Fe $3d$ magnetic moments to orbital-selective localization.

However, we note that the calculated critical pressure of the MIT $\sim$85 GPa in the $P2_1/n$ phase (neglecting a structural change at the MIT) of $CaFeO_3$ is significantly, by almost three times, higher than that found in the experiments [7]. It is know experimentally that the MIT in $CaFeO_3$ is accompanied by a structural change to the orthorhombic *Pbnm* phase [7–10]. In agreement with this, our DFT+DMFT total-energy calculations show that upon compression to $\sim 0.83V_0$, the $P2_1/n$ lattice becomes energetically unfavorable, with the orthorhombic *Pbnm* phase being thermodynamically stable. We therefore conclude that above $p_c \sim 41$ GPa, $CaFeO_3$ undergoes a phase transition from a monoclinic $P2_1/n$ to the orthorhombic *Pbnm* crystal structure (see Fig. 1). We note, however, that this value should be considered as an upper-bound estimate because of neglecting the pressure-induced atomic displacements upon fitting the DFT+DMFT total-energy results to the third-order Birch-Murnaghan equation of states. In agreement with this, a large reduction of p_c upon taking into account a change of the crystal structure suggests a crucial role of the coupling between electronic correlations and lattice, in agreement with the behavior of nickelates [18–27].

E. Electronic structure and spin state of iron in *Pbnm* $CaFeO_3$

In agreement with experiment, the phase transition is accompanied by metallization of $CaFeO_3$. Interestingly, the calculated local magnetic moments for the *Pbnm* phase are nearly equal to that in the highly compressed metallic $P2_1/n$ phase of $CaFeO_3$, $\sim$2.22 μ_B at $\sim 0.7V_0$. The phase transition is accompanied by a remarkable collapse of the unit-cell volume of $\frac{\Delta V}{V} \sim 4\%$ and results in suppression of the cooperative breathing mode distortion of the lattice. In fact, in the *Pbnm* phase Fe sites have a regular oxygen coordination with no evidence for charge disproportionation. We also note that the charge-disproportionated state is found to be unstable within our DFT+DMFT calculations for the *Pbnm* lattice. The calculated bulk modulus for the high-pressure *Pbnm* phase is about 197 GPa. This suggests that the $P2_1/n$ to *Pbnm* phase transition is accompanied by a remarkable *increase* of the bulk modulus upon the pressure-induced insulator-to-metal phase transition, implying a crucial importance of the interplay of electronic correlations and the lattice to explain the properties of $CaFeO_3$.

Our analysis of the atomic spin state configurations and local spin susceptibilities shows that the phase transition is associated with a spin state transition accompanied by a significant delocalization of the Fe $3d$ states (see Figs. 4 and 5). In particular, in the metallic *Pbnm* phase at 93 GPa (i.e., above the MIT) the Fe ions adopt the IS state with a predominant weight of $\sim$56%, with a strong admixture $\sim$34% of the low-spin state. Our analysis of fluctuating valence state of the Fe ions yields a predominant contribution of the $3d^5$ configuration, $\sim$47%, with a considerable admixture of the $3d^4$ and $3d^6$ states of $\sim$ 34% and 16%, respectively. This implies that the electronic state of the Fe ions in the *Pbnm* phase consists of heavily mixed $d^5\underline{L}$ and d^4 states, highlighting negative charge transfer due to strong covalency in $CaFeO_3$. We therefore identify the metallic *Pbnm* phase of $CaFeO_3$ as a negative charge transfer material with a local Fe $3d^{5-\delta}\underline{L}^{1-\delta}$ electron configuration (with $\delta \ll 1$), implying the important role of Fe $3d$ to O $2p$ negative charge transfer.

F. Spectral function and quasiparticle weights

The MIT transition results in a significant redistribution of the spectral weight near the Fermi level. It leads to the formation of a quasiparticle peak originating from the Fe t_{2g} states with the lower and upper Hubbard bands located at -1.2 eV and 1.5 eV, respectively (see the right panel of Fig. 3). It gives a strong depopulation of the Fe e_g orbital occupations. Thus, the Fe e_g orbital occupations change from 0.38 (at ambient pressure in the *Pbnm* phase) to 0.17 per spin orbit under pressure increase to 93 GPa. On the other hand, it results in a gradual increase of the Fe t_{2g} occupations, while the total Wannier Fe $3d$ occupation in the *Pbnm* phase remains essentially unchanged with pressure, ∼4.73. We note that this value nearly equals the average Wannier Fe $3d$ total occupancy of the Fe ions in the metallic $P2_1/n$ phase.

The *Pbnm* phase of $CaFeO_3$ is a strongly correlated metal, characterized by a Fermi-liquid-like behavior with a large orbital-dependent damping of $\mathrm{Im}[\Sigma(\omega)] \sim 0.52$ and 0.09 eV for the Fe t_{2g} and e_g quasiparticle states at the Fermi energy, at about 93 GPa. The latter indicates strong incoherence of the Fe $3d$ electronic states caused by proximity of the $3d$ state to orbital-selective localization. We evaluate the quasiparticle mass enhancement $\frac{m^*}{m} = 1 - \partial \mathrm{Im}\Sigma(\omega)/\partial\omega|_{\omega=0}$ using extrapolation of the self-energy $\Sigma(\omega)$ to $\omega = 0$ eV, which gives a quantitative measure of the correlation strength. At 93 GPa we obtain $m^*/m \sim 5.0$ and 1.7 for the Fe t_{2g} and e_g bands, respectively. We also note that similarly to the insulating $P2_1/n$ phase the *Pbnm* phase of $CaFeO_3$ exhibits a remarkable collapse of the local magnetic moments under pressure at about 43 GPa (which is almost equal to the critical pressure p_c of the $P2_1/n$ to *Pbnm* structural transition). This implies that the $P2_1/n$ to *Pbnm* phase transition is accompanied by a collapse of the local magnetic moments of the Fe ions.

Overall, our results for the electronic structure, spin and charge state of Fe ions, and phase stability of $CaFeO_3$ under pressure agree well with available experimental studies. Our DFT+DMFT calculations give a microscopic understanding of the pressure-induced evolution of the electronic structure and lattice properties of $CaFeO_3$. It reveals the complex interplay between the electronic correlations and lattice effects in the vicinity of a pressure-induced MIT in $CaFeO_3$. We note that our results are compatible with the scenario of bond disproportionation, which comprises the "compressed" Fe A $3d^{5-\delta}\underline{L}^{2-\delta}$ and "expanded" Fe B $3d^5$ sites with $\delta \ll 1$ alternating in the insulating $P2_1/n$ phase and a homogeneous Fe $3d^{5-\delta}\underline{L}^{1-\delta}$ state in the metallic *Pbnm* phase. This implies the key role of the coupling between electronic correlations, negative charge transfer effects, and the lattice, in close similarity to the behavior rare-earth nickelates $RNiO_3$ [18–27].

IV. CONCLUSION

In conclusion, we employed the DFT+DMFT computational approach to study the effects of electronic correlations on the electronic structure, spin and charge state of Fe ions, and structural phase stability of *paramagnetic* $CaFeO_3$ across the pressure-induced insulator-to-metal phase transition. In agreement with experiments, the DFT+DMFT calculations show that at low pressure and temperature $CaFeO_3$ is a negative charge transfer insulator characterized by strong localization of the Fe $3d$ electrons. It crystallizes in the monoclinic $P2_1/n$ crystal structure with a cooperative breathing mode distortion of the lattice. While our analysis of the Fe $3d$ Wannier occupations and local moments for the insulating $P2_1/n$ phase give a robust charge disproportionation, a charge difference evaluated as an integral of the charge density around the structurally distinct Fe A and Fe B ions is rather weak, ∼0.04. This implies the importance of the Fe $3d$ and O $2p$ negative charge transfer and supports the formation of a bond-disproportionated state characterized by the Fe $3d^{5-\delta}\underline{L}^{2-\delta}$ and $3d^5$ valence configurations with $\delta \ll 1$ for the "compressed" Fe A and "expanded" Fe B sites, respectively, in the insulating phase of $CaFeO_3$. This behavior is consistent with a substantial Fe-O covalence and strong hybridization between the unoccupied Fe e_g and O $2p$ states.

In agreement with experiment, above critical pressure of ∼41 GPa $CaFeO_3$ undergoes the insulator-to-metal phase transition which is accompanied by a structural transformation into the orthorhombic *Pbnm* phase. The phase transition is accompanied by suppression of the cooperative breathing mode distortion of the lattice and, hence, results in the melting of bond disproportionation of the Fe ions. Our analysis suggests that the MIT transition is accompanied by orbital-dependent delocalization of the Fe $3d$ electrons and leads to a remarkable collapse of the local magnetic moments. Our results imply the crucial importance of the interplay of electronic correlations and structural effects to explain the electronic properties and structural phase equilibrium of $CaFeO_3$. Our findings highlight the subtle interplay between electronic correlations, charge transfer effects, and structural phase stability in a negative charge transfer material $CaFeO_3$ across the pressure-induced MIT. We believe that this topic deserves further detailed theoretical and experimental considerations.

ACKNOWLEDGMENTS

We acknowledge support by the Russian Foundation for Basic Research (Project No. 20-42-660027). The theoretical analysis of the electronic structure and DFT calculations were supported by the state assignment of Minobrnauki of Russia (theme "Electron" No. AAAA-A18-118020190098-5).

[1] N. F. Mott, *Metal-Insulator Transitions* (Taylor & Francis, London, 1990).
[2] M. Imada, A. Fujimori, and Y. Tokura, Rev. Mod. Phys. **70**, 1039 (1998).
[3] Y. Tokura and N. Nagaosa, Science **288**, 462 (2000).
[4] E. Dagotto, T. Hotta, and A. Moreo, Phys. Rep. **344**, 1 (2001).
[5] M. B. Salamon and M. Jaime, Rev. Mod. Phys. **73**, 583 (2001).
[6] Y. Tokura, S. Seki, and N. Nagaosa, Rep. Prog. Phys. **77**, 076501 (2014).
[7] M. Takano, S. Nasu, T. Abe, K. Yamamoto, S. Endo, Y. Takeda, and J. B. Goodenough, Phys. Rev. Lett. **67**, 3267 (1991).

[8] A. E. Bocquet, A. Fujimori, T. Mizokawa, T. Saitoh, H. Namatame, S. Suga, N. Kimizuka, Y. Takeda, and M. Takano, Phys. Rev. B **45**, 1561 (1992).

[9] P. M. Woodward, D. E. Cox, E. Moshopoulou, A. W. Sleight, and S. Morimoto, Phys. Rev. B **62**, 844 (2000).

[10] T. Takeda, R. Kanno, Y. Kawamoto, M. Takano, S. Kawasaki, T. Kamiyama, and F. Izum, Solid State Sci. **2**, 673 (2000).

[11] G. Catalan, Phase Transit. **81**, 729 (2008).

[12] S. Middey, J. Chakhalian, P. Mahadevan, J. W. Freeland, A. J. Millis, and D. D. Sarma, Annu. Rev. Mater. Res. **46**, 305 (2016).

[13] S. Catalano, M. Gibert, J. Fowlie, J. Íñiguez, J.-M. Triscone, and J. Kreisel, Rep. Prog. Phys. **81**, 046501 (2018).

[14] J. Zaanen, G. A. Sawatzky, and J. W. Allen, Phys. Rev. Lett. **55**, 418 (1985).

[15] I. I. Mazin, D. I. Khomskii, R. Lengsdorf, J. A. Alonso, W. G. Marshall, R. M. Ibberson, A. Podlesnyak, M. J. Martínez-Lope, and M. M. Abd-Elmeguid, Phys. Rev. Lett. **98**, 176406 (2007).

[16] J. B. Torrance, P. Lacorre, A. I. Nazzal, E. J. Ansaldo, and C. Niedermayer, Phys. Rev. B **45**, 8209(R) (1992).

[17] J. L. García-Muñoz, J. Rodríguez-Carvajal, P. Lacorre, and J. B. Torrance, Phys. Rev. B **46**, 4414 (1992).

[18] H. Park, A. J. Millis, and C. A. Marianetti, Phys. Rev. Lett. **109**, 156402 (2012).

[19] S. Johnston, A. Mukherjee, I. Elfimov, M. Berciu, and G. A. Sawatzky, Phys. Rev. Lett. **112**, 106404 (2014).

[20] H. Park, A. J. Millis, and C. A. Marianetti, Phys. Rev. B **89**, 245133 (2014).

[21] A. Subedi, O. E. Peil, and A. Georges, Phys. Rev. B **91**, 075128 (2015).

[22] V. Bisogni, S. Catalano, R. J. Green, M. Gibert, R. Scherwitzl, Y. Huang, V. N. Strocov, P. Zubko, S. Balandeh, J.-M. Triscone, G. Sawatzky, and T. Schmitt, Nat. Commun. **7**, 13017 (2016).

[23] A. Hampel and C. Ederer, Phys. Rev. B **96**, 165130 (2017).

[24] K. Haule and G. L. Pascut, Sci. Rep. **7**, 10375 (2017).

[25] A. Hampel, P. Liu, C. Franchini, and C. Ederer, npj Quantum Mater. **4**, 5 (2019).

[26] A. B. Georgescu, O. E. Peil, A. S. Disa, A. Georges, and A. J. Millis, Proc. Natl. Acad. Sci. USA **116**, 14434 (2019).

[27] O. E. Peil, A. Hampel, C. Ederer, and A. Georges, Phys. Rev. B **99**, 245127 (2019).

[28] S. Ishiwata, M. Azuma, M. Takano, E. Nishibori, M. Takata, M. Sakatac, and K. Kato, J. Mater. Chem. **12**, 3733 (2002).

[29] M. Azuma, S. Carlsson, J. Rodgers, M. G. Tucker, M. Tsujimoto, S. Ishiwata, S. Isoda, Y. Shimakawa, M. Takano, and J. P. Attfield, J. Am. Chem. Soc. **129**, 14433 (2007).

[30] S. J. E. Carlsson, M. Azuma, Y. Shimakawa, M. Takano, A. Hewat, and J. P. Attfield, J. Solid State Chem. **181**, 611 (2008).

[31] M. Azuma, W. Chen, H. Seki, M. Czapski, O. Smirnova, O. Kengo, M. Mizumaki, T. Watanuki, N. Ishimatsu, N. Kawamura, S. Ishiwata, M. G. Tucker, Y. Shimakawa, and J. P. Attfield, Nat. Commun. **2**, 347 (2011).

[32] K. Oka, M. Mizumaki, C. Sakaguchi, A. Sinclair, C. Ritter, J. P. Attfield, and M. Azuma, Phys. Rev. B **88**, 014112 (2013).

[33] A. Paul, A. Mukherjee, I. Dasgupta, A. Paramekanti, and T. Saha-Dasgupta, Phys. Rev. Lett. **122**, 016404 (2019).

[34] I. Leonov, A. S. Belozerov, and S. L. Skornyakov, Phys. Rev. B **100**, 161112(R) (2019).

[35] T. Tsuchiya, H. Saito, M. Yoshida, T. Katsumata, T. Ohba, Y. Inaguma, T. Tsurui, and M. Shikano, Mater. Res. Soc. Symp. Proc. **988**, 9880916 (2006).

[36] X. Ye, J. Zhao, H. Das, D. Sheptyakov, J. Yang, Y. Sakai, H. Hojo, Z. Liu, L. Zhou, L. Cao, T. Nishikubo, S. Wakazaki, C. Dong, X. Wang, Z. Hu, H.-J. Lin, C.-T. Chen, C. Sahle, A. Efiminko, H. Cao *et al.*, Nat. Commun. **12**, 1917 (2021).

[37] Y. Sakai, J. Yang, R. Yu, H. Hojo, I. Yamada, P. Miao, S. Lee, S. Torii, T. Kamiyama, M. Ležaić, G. Bihlmayer, M. Mizumaki, J. Komiyama, T. Mizokawa, H. Yamamoto, T. Nishikubo, Y. Hattori, K. Oka, Y. Yin, J. Dai, W. Li *et al.*, J. Am. Chem. Soc. **139**, 4574 (2017).

[38] Z. Liu, Y. Sakai, J. Yang, W. Li, Y. Liu, X. Ye, S. Qin, J. Chen, S. Agrestini, K. Chen, S.-C. Liao, S.-C. Haw, F. Baudelet, H. Ishii, T. Nishikubo, H. Ishizaki, T. Yamamoto, Z. Pan, M. Fukuda, K. Ohashi *et al.*, J. Am. Chem. Soc. **142**, 5731 (2020).

[39] A. Hariki, K.-H. Ahn, and J. Kuneš, Phys. Rev. B **104**, 235101 (2021).

[40] W. M. Xu, O. Naaman, G. Rozenberg, M. P. Pasternak, and R. D. Taylor, Phys. Rev. B **64**, 094411 (2001).

[41] M. V. Patrakeev, J. A. Bahteeva, E. B. Mitberg, I. A. Leonidov, V. L. Kozhevnikov, and K. R. Poeppelmeier, J. Solid State Chem. **172**, 219 (2003).

[42] V. R. Galakhov, E. Z. Kurmaev, K. Kuepper, M. Neumann, J. A. McLeod, A. Moewes, I. A. Leonidov, and V. L. Kozhevnikov, J. Phys. Chem. C **114**, 5154 (2010).

[43] J. Fujioka, S. Ishiwata, Y. Kaneko, Y. Taguchi, and Y. Tokura, Phys. Rev. B **85**, 155141 (2012).

[44] P. C. Rogge, R. U. Chandrasena, A. Cammarata, R. J. Green, P. Shafer, B. M. Lefler, A. Huon, A. Arab, E. Arenholz, H. N. Lee, T.-L. Lee, S. Nemšák, J. M. Rondinelli, A. X. Gray, and S. J. May, Phys. Rev. Mater. **2**, 015002 (2018).

[45] P. C. Rogge, R. J. Green, R. Sutarto, and S. J. May, Phys. Rev. Mater. **3**, 084404 (2019).

[46] S. Jana, S. K. Panda, D. Phuyal, B. Pal, S. Mukherjee, A. Dutta, P. A. Kumar, D. Hedlund, J. Schött, P. Thunström, Y. Kvashnin, H. Rensmo, M. V. Kamalakar, Carlo U. Segre, P. Svedlindh, K. Gunnarsson, S. Biermann, O. Eriksson, O. Karis, and D. D. Sarma, Phys. Rev. B **99**, 075106 (2019).

[47] L. Wang, Y. Du, P. V. Sushko, M. E. Bowden, K. A. Stoerzinger, S. M. Heald, M. D. Scafetta, T. C. Kaspar, and S. A. Chambers, Phys. Rev. Mater. **3**, 025401 (2019).

[48] M. Onose, H. Takahashi, H. Sagayama, Y. Yamasaki, and S. Ishiwata, Phys. Rev. Mater. **4**, 114420 (2020).

[49] I. R. Shein, K. I. Shein, V. L. Kozhevnikov, and A. L. Ivanovskii, Phys. Solid State **47**, 2082 (2005).

[50] T. Saha-Dasgupta, Z. S. Popović, and S. Satpathy, Phys. Rev. B **72**, 045143 (2005).

[51] V. E. Alexandrov, E. A. Kotomin, J. Maier, and R. A. Evarestov, J. Chem. Phys. **129**, 214704 (2008).

[52] A. Cammarata and J. M. Rondinelli, Phys. Rev. B **86**, 195144 (2012); **87**, 155135 (2013).

[53] Y. Zhang, M. M. Schmitt, A. Mercy, J. Wang, and P. Ghosez, Phys. Rev. B **98**, 081108(R) (2018).

[54] G. M. Dalpian, Q. Liu, J. Varignon, M. Bibes, and A. Zunger, Phys. Rev. B **98**, 075135 (2018).

[55] J. Varignon, M. Bibes, and A. Zunger, Nat. Commun. **10**, 1658 (2019).

[56] J. Varignon, M. Bibes, and A. Zunger, Phys. Rev. B **100**, 035119 (2019).

[57] V. I. Anisimov, J. Zaanen, and O. K. Andersen, Phys. Rev. B **44**, 943 (1991).

[58] A. I. Liechtenstein, V. I. Anisimov, and J. Zaanen, Phys. Rev. B **52**, R5467 (1995).

[59] J. Sun, A. Ruzsinszky, and J. P. Perdew, Phys. Rev. Lett. **115**, 036402 (2015).

[60] M. E. Merkel and C. Ederer, Phys. Rev. B **104**, 165135 (2021).

[61] W. Metzner and D. Vollhardt, Phys. Rev. Lett. **62**, 324 (1989).

[62] A. Georges, G. Kotliar, W. Krauth, and M. J. Rozenberg, Rev. Mod. Phys. **68**, 13 (1996).

[63] G. Kotliar, S. Y. Savrasov, K. Haule, V. S. Oudovenko, O. Parcollet, and C. A. Marianetti, Rev. Mod. Phys. **78**, 865 (2006).

[64] V. I. Anisimov, A. I. Poteryaev, M. A. Korotin, A. O. Anokhin, and G. Kotliar, J. Phys.: Condens. Matter **9**, 7359 (1997).

[65] K. Haule, Phys. Rev. B **75**, 155113 (2007).

[66] L. V. Pourovskii, B. Amadon, S. Biermann, and A. Georges, Phys. Rev. B **76**, 235101 (2007).

[67] B. Amadon, F. Lechermann, A. Georges, F. Jollet, T. O. Wehling, and A. I. Lichtenstein, Phys. Rev. B **77**, 205112 (2008).

[68] M. Aichhorn, L. Pourovskii, V. Vildosola, M. Ferrero, O. Parcollet, T. Miyake, A. Georges, and S. Biermann, Phys. Rev. B **80**, 085101 (2009).

[69] I. Leonov, Phys. Rev. B **92**, 085142 (2015).

[70] I. Leonov, V. I. Anisimov, and D. Vollhardt, Phys. Rev. B **91**, 195115 (2015).

[71] I. Leonov, A. O. Shorikov, V. I. Anisimov, and I. A. Abrikosov, Phys. Rev. B **101**, 245144 (2020).

[72] I. Leonov, S. L. Skornyakov, V. I. Anisimov, and D. Vollhardt, Phys. Rev. Lett. **115**, 106402 (2015).

[73] G. Lantz, M. Hajlaoui, E. Papalazarou, V. L. R. Jacques, A. Mazzotti, M. Marsi, S. Lupi, M. Amati, L. Gregoratti, L. Si, and Z. Zhong, and K. Held, Phys. Rev. Lett. **115**, 236802 (2015).

[74] Z. Zhong, M. Wallerberger, J. M. Tomczak, C. Taranto, N. Parragh, A. Toschi, G. Sangiovanni, and K. Held, Phys. Rev. Lett. **114**, 246401 (2015).

[75] I. Leonov, L. Pourovskii, A. Georges, and I. A. Abrikosov, Phys. Rev. B **94**, 155135 (2016).

[76] S. Backes, T. C. Rödel, F. Fortuna, E. Frantzeskakis, P. Le Févre, F. Bertran, M. Kobayashi, R. Yukawa, T. Mitsuhashi, M. Kitamura, K. Horiba, H. Kumigashira, R. Saint-Martin, A. Fouchet, B. Berini, Y. Dumont, A. J. Kim, F. Lechermann, H. O. Jeschke, M. J. Rozenberg, R. Valentí *et al.*, Phys. Rev. B **94**, 241110(R) (2016).

[77] L. de' Medici, Phys. Rev. Lett. **118**, 167003 (2017).

[78] P. Seth, O. E. Peil, L. Pourovskii, M. Betzinger, C. Friedrich, O. Parcollet, S. Biermann, F. Aryasetiawan, and A. Georges, Phys. Rev. B **96**, 205139 (2017).

[79] J. I. Facio, J. Mravlje, L. Pourovskii, P. S. Cornaglia, and V. Vildosola, Phys. Rev. B **98**, 085121 (2018).

[80] S. L. Skornyakov, V. I. Anisimov, D. Vollhardt, and I. Leonov, Phys. Rev. B **96**, 035137 (2017).

[81] F. Lechermann, N. Bernstein, I. I. Mazin, and R. Valentí, Phys. Rev. Lett. **121**, 106401 (2018).

[82] P. Villar Arribi and L. de' Medici, Phys. Rev. Lett. **121**, 197001 (2018).

[83] S. L. Skornyakov, V. I. Anisimov, D. Vollhardt, and I. Leonov, Phys. Rev. B **97**, 115165 (2018).

[84] F. Lechermann, W. Körner, D. F. Urban, and C. Elsässer, Phys. Rev. B **100**, 115125 (2019).

[85] B. G. Jang, J. Liu, Q. Hu, K. Haule, H.-K. Mao, W. L. Mao, D. Y. Kim, and J. H. Shim, Phys. Rev. B **100**, 014418 (2019).

[86] S. Mandal, K. Haule, K. M. Rabe, and D. Vanderbilt, Phys. Rev. B **100**, 245109 (2019).

[87] E. Koemets, I. Leonov, M. Bykov, E. Bykova, S. Chariton, G. Aprilis, T. Fedotenko, S. Clément, J. Rouquette, J. Haines, V. Cerantola, K. Glazyrin, C. McCammon, V. B. Prakapenka, M. Hanfland, H.-P. Liermann, V. Svitlyk, R. Torchio, A. D. Rosa, T. Irifune *et al.*, Phys. Rev. Lett. **126**, 106001 (2021).

[88] I. Leonov and S. Biermann, Phys. Rev. B **103**, 165108 (2021).

[89] S. Bhandary and K. Held, Phys. Rev. B **103**, 245116 (2021).

[90] S. L. Skornyakov, V. I. Anisimov, and I. Leonov, Phys. Rev. B **103**, 155115 (2021).

[91] E. Greenberg, I. Leonov, S. Layek, Z. Konopkova, M. P. Pasternak, L. Dubrovinsky, R. Jeanloz, I. A. Abrikosov, and G. K. Rozenberg, Phys. Rev. X **8**, 031059 (2018).

[92] I. Leonov, G. Kh. Rozenberg, and I. A. Abrikosov, npj Comput. Mater. **5**, 90 (2019).

[93] A. Georges, L. de'Medici, and J. Mravlje, Annu. Rev. Condens. Matter Phys. **4**, 137 (2013).

[94] J. Kuneš and V. Křápek, Phys. Rev. Lett. **106**, 256401 (2011).

[95] A. Isidori, M. Berović, L. Fanfarillo, L. de'Medici, M. Fabrizio, and M. Capone, Phys. Rev. Lett. **122**, 186401 (2019).

[96] A. Richaud, M. Ferraretto, and M. Capone, Phys. Rev. B **103**, 205132 (2021).

[97] P. Giannozzi, S. Baroni, N. Bonini, M. Calandra, R. Car, C. Cavazzoni, D. Ceresoli, G. L. Chiarotti, M. Cococcioni, I. Dabo *et al.*, J. Phys.: Condens. Matter **21**, 395502 (2009).

[98] F. D. Murnaghan, Proc. Natl. Acad. Sci. USA **30**, 244 (1944).

[99] F. Birch, Phys. Rev. **71**, 809 (1947).

[100] N. Marzari, A. A. Mostofi, J. R. Yates, I. Souza, and D. Vanderbilt, Rev. Mod. Phys. **84**, 1419 (2012).

[101] V. I. Anisimov, D. E. Kondakov, A. V. Kozhevnikov, I. A. Nekrasov, Z. V. Pchelkina, J. W. Allen, S.-K. Mo, H.-D. Kim, P. Metcalf, S. Suga, A. Sekiyama, G. Keller, I. Leonov, X. Ren, and D. Vollhardt, Phys. Rev. B **71**, 125119 (2005).

[102] G. Trimarchi, I. Leonov, N. Binggeli, D. Korotin, and V. I. Anisimov, J. Phys.: Condens. Matter **20**, 135227 (2008).

[103] We note that upon construction of the Wannier functions, we perform orthonormalization of the Fe 3*d* and O 2*p* Wannier orbitals to guarantee that these states are orthogonal. For $CaFeO_3$ it results in the Wannier band structure which is identical to the Fe 3*d* and O 2*p* eigenvalues of the DFT Hamiltonian in the Bloch basis set in the energy window of the Fe 3*d* and O 2*p* states. Using different energy windows for the Fe 3*d* and O 2*p* states allows us to decrease the Fe 3*d*–O 2*p* hybridization strength, which partly solves the "overbinding" problem (too large Fe 3*d* Wannier occupation due to *p*-*d* charge transfer) of the standard Wannier projection scheme with the same (overlapping) energy windows for the Fe 3*d* and O 2*p* states.

[104] E. Gull, A. J. Millis, A. I. Lichtenstein, A. N. Rubtsov, M. Troyer, and P. Werner, Rev. Mod. Phys. **83**, 349 (2011).

[105] J. P. Perdew, K. Burke, and M. Ernzerhof, Phys. Rev. Lett. **77**, 3865 (1996).

[106] A. D. Corso, Comput. Mater. Sci. **95**, 337 (2014).

[107] K. Lejaeghere, G. Bihlmayer, B. Björkman, P. Blaha, S. Blügel, V. Blum, G. Caliste, I. E. Castelli, S. J. Clark, A. Dal Corso *et al.*, Science **351**, 1415 (2016).
[108] G. Prandini, A. Marrazzo, I. E. Castelli, N. Mounet, and N. Marzari, npj Comput. Mater. **4**, 72 (2018).
[109] K. F. Garrity, J. W. Bennett, K. M. Rabe, and D. Vanderbilt, GBRV High-Throughput Pseudopotentials, http://physics.rutgers.edu/gbrv.
[110] F. C. Zhang and T. M. Rice, Phys. Rev. B **37**, 3759 (1988).
[111] J. P. Wright, J. P. Attfield, and P. G. Radaelli, Phys. Rev. B **66**, 214422 (2002).
[112] I. Leonov, A. N. Yaresko, V. N. Antonov, and V. I. Anisimov, Phys. Rev. B **74**, 165117 (2006).
[113] H.-T. Jeng, G. Y. Guo, and D. J. Huang, Phys. Rev. B **74**, 195115 (2006).
[114] I. Leonov, A. N. Yaresko, V. N. Antonov, J. P. Attfield, and V. I. Anisimov, Phys. Rev. B **72**, 014407 (2005).
[115] M. S. Senn, J. P. Wright, and J. P. Attfield, Nature (London) **481**, 173 (2012).
[116] G. Perversi, E. Pachoud, J. Cumby, J. M. Hudspeth, J. P. Wright, S. A. J. Kimber, and J. P. Attfield, Nat. Commun. **10**, 2857 (2019).